40th AIAA/ASME/SAE/ASEE Joint Propulsion Conference and Exhibit, July 11-14, 2004, Fort Lauderdale, FL

# The Effect of Transient Nozzle Flow on Detonation Tube Impulse

M. Cooper* and J. E. Shepherd†

*California Institute of Technology, Pasadena, CA, 91125, USA*

**Impulse generation with gaseous detonation requires conversion of chemical energy into mechanical energy. Because of the poor performance of straight detonation tubes compared to conventional propulsion systems and the success of using nozzles on rocket engines, the effect of nozzles on detonation tubes is being investigated. The first experimental investigation measuring impulse by gaseous detonation in tubes with nozzles operating in varying environment pressures using the ballistic pendulum technique is presented. Converging, diverging, and converging-diverging nozzles were tested to determine the effect of divergence angle, nozzle length, and volumetric fill fraction on impulse. The largest increases in specific impulse, 72% at an environment pressure of 100 kPa and 43% at an environment pressure of 1.4 kPa, were measured with the largest diverging nozzle tested that had a 12° half angle and a length of 0.6 m. There are two regimes of nozzle operation depending on the environment pressure that is observed from these data. The experimental data are compared to calculations of the impulse obtained by steady flow expansion through the nozzle with finite rate kinetics.**

## Nomenclature

| | |
|---|---|
| $\alpha$ | nozzle half angle |
| $\beta$ | model constant equal to 0.53 for original impulse model[1] |
| $\beta_{LP}$ | variable model constant for modified impulse model[2] |
| $\mathbf{\Omega}$ | matrix of species reaction rates |
| $\mathbf{Y}$ | matrix of species mass fractions |
| $\dot{\sigma}$ | thermicity |
| $\dot{m}$ | mass flow rate |
| $\gamma$ | ratio of specific heats |
| $\overline{u_x}$ | measured average gas velocity at nozzle exit |
| $\rho$ | density |
| $A$ | area |
| $A_x$ | area of nozzle exit |
| $C$ | mass of explosive mixture in detonation tube |
| $c$ | sound speed |
| $F$ | force |
| $g$ | gravitational acceleration |

*Graduate student, Aeronautics, 1200 E. California Boulevard, MC 205-45, Pasadena, CA, 91125.

†Professor, Aeronautics, 1200 E. California Boulevard, MC 105-50, Pasadena, CA, 91125.

| | |
|---|---|
| $h$ | specific enthalpy |
| $h_t$ | total specific enthalpy |
| $I$ | impulse |
| $I_{sp}$ | mixture-based specific impulse |
| $M$ | Mach number |
| $N$ | mass of inert gas tamper in detonation tube |
| $n$ | ratio of explosive mixture density to inert gas density |
| $P$ | pressure |
| $P_0$ | environment pressure |
| $P_3$ | state 3 pressure behind Taylor wave |
| $P_i$ | pressure at inlet of steady flow nozzle |
| $P_x$ | pressure at exit of steady flow nozzle |
| $R$ | gas constant |
| $R_0$ | detonation tube radius |
| $T$ | temperature |
| $t$ | time |
| $T_i$ | temperature at nozzle inlet |
| $u$ | velocity |
| $u_i$ | velocity at nozzle inlet |
| $u_x$ | gas velocity at nozzle exit |
| $V$ | volume |
| $x$ | distance |
| $\mathcal{M}$ | mass in control volume |
| $\mathcal{W}$ | molar mass of product gases |

# I. Introduction

Nozzles are well known to expand the exhaust flow in steady devices, thus, increasing the impulse over that of devices without nozzles. In unsteady devices, such as detonation tubes, the effect of nozzles are not well understood nor has been previously investigated experimentally. This work presents the results of an experimental study that directly measures the single-cycle impulse from detonation tubes with diverging nozzles. Presented here is the third part of an experimental and analytical study investigating impulse generation in detonation tubes.[2] The first part of Cooper[2] consolidated the available data of partially filled detonation tubes in cylindrical geometries to illustrate the correlation between the explosive mass fraction within the tube and the specific impulse. As the explosive mass fraction decreases, the specific impulse increases due to the tamping effect of the inert gas filling the tube that is not considered when calculating the specific impulse. It was analytically proven that a limiting value for the specific impulse exists in a nearly empty tube and depends on the interface properties between the hot products and the inert mixture. The second part of Cooper[2] carried out an experimental study to directly measure the single-cycle impulse from a fully filled detonation tube with no exit nozzle as a function of environment pressure. As expected, the impulse increases as the environment pressure decreases which can be attributed to the increased pressure differential across the thrust surface and the increased exhaust gas blow down time. From the experimental data, the impulse model of Wintenberger et al.[1] was modified to include a new variable model parameter $\beta_{LP} \propto P_3/P_0$ that replaces the previous constant model parameter $\beta = 0.53$. The modified impulse model[2]

$$I_{sp} = \frac{I}{V\rho_1 g} = \frac{(P_3 - P_0)}{\rho_1 g U_{CJ}} \left[ \frac{(P_3 - P_1)}{(P_3 - P_0)} + \alpha \frac{U_{CJ}}{c_3} + \beta_{LP} \frac{U_{CJ}}{c_3} \right] \tag{1}$$

is capable of predicting the single-cycle impulse in simplified detonation tubes for a variety of initial pressures, dilutions, equivalence ratios, and now environment pressures.

Comparisons of the impulse data from fully filled detonation tubes to steady flow impulse predictions

based on steady, adiabatic expansion showed that the exhaust products from a straight tube are underexpanded. This lack of product gas expansion results[2] in significant decreases in impulse from the ideal case, especially for pressure ratios $P_3/P_0 > 10$. In an effort to promote additional gas expansion and hopefully recover some of the lost energy, experiments with conical converging nozzles, conical diverging nozzles, and conical converging-diverging nozzles were carried out.

Previous experimental and numerical studies have investigated the effects of nozzles on detonation tubes. The first study was carried out by Cambier and and Tegner[3] who numerically studied contoured diverging nozzles on detonation tubes. The effect on the impulse was quantified in hydrogen-oxygen mixtures at 1 atm and 350 K. Eidelman and Yang[4] carried out numerical calculations to study the effect of converging and diverging nozzles on tubes with a 6 cm inner diameter and a length of 15 cm in acetylene-air mixtures at 1 atm pressure. The nozzles contained air at standard conditions. The converging nozzles were found to cause multiple shock reflections and longer blow down times. A relatively long converging nozzle with a small half angle increased the impulse over the baseline case of a plain tube, but this is most likely due to the partial fill effect. Very short converging nozzles showed no significant increase in impulse. Two conical diverging nozzles and a bell shaped nozzle with an area ratio of 5, designed for full expansion to atmospheric conditions, were examined. However, the flow overexpanded in the bell shaped nozzle and decreased the impulse below the ideal value.

Yang et al.[5] carried out numerical calculations studying the impulse for a converging, diverging, and plug nozzle in hydrogen-air mixtures at 0.29 atm and 228 K. The nozzle contained air at the same conditions. The conical converging and diverging nozzles had 10° half angles and area ratios of $A_{exit}/A_{tube}$ of 1.25 and 0.75, respectively. They observed a limited performance gain with the diverging nozzle over the case of a straight extension.

Guzik et al.[6] carried out a numerical study using the method of characteristics to solve the flow field within a detonation tube containing a fixed area nozzle and a variable area nozzle. They assume the detonation products for the propane-oxygen mixture, initially at 1 atm and 295 K, are frozen at the Chapman-Jouguet equilibrium conditions. The variable area nozzle was a diverging nozzle with "flexible" cross section in order to fully expand the flow. The fixed area nozzle had an exit area equal to the tube cross-sectional area and a converging-diverging throat section. For a detonation initiated at the thrust surface, they found that the optimum area ratio $A_{throat}/A_{tube}$ was 0.54. The throat restriction was observed to delay the time at which the maximum impulse was observed over that of the plain tube. They concluded that a variable nozzle can always be added to extract more thrust. These results are compared to the results of other 0-D, 1-D, and 2-D models as discussed in Harris et al.[7]

Morris[8] carried out a numerical investigation using a quasi-one-dimensional, finite-rate chemistry computational fluid dynamics model for pulse detonation rocket engines in hydrogen-oxygen mixtures. Four different geometries were analyzed including a plain detonation tube, a straight extension, and two converging-diverging nozzles with different throat restrictions. The converging and diverging sections had 15° half angles. The converging-diverging nozzles were found to always be more effective than a straight extension at increasing the impulse for initial pressure ratios $P_1/P_0$ between 10 and 1000.

Cooper et al.[9] previously carried out an experimental investigation measuring impulse from a 1 m long detonation tube exhausting into atmospheric air with a conical diverging nozzle. The nozzle had a length of 0.3 m and an 8° half angle. The impulse measurements were obtained in ethylene-oxygen mixtures at 100 kPa initial pressure with different nitrogen dilutions. A ballistic pendulum arrangement was used and the tube contained internal obstacles to promote deflagration to detonation transition in the diluted mixtures. A constant increase in impulse of approximately 1% over the plain tube case was observed for nitrogen dilutions between 0% and 40%.

Falempin et al.[10] experimentally investigated the effect of diverging nozzles on impulse with a ballistic pendulum arrangement in ethylene-oxygen mixtures. They tested conical diverging nozzles, bell shaped nozzles, and straight extensions. The nozzles contained air at ambient conditions and they attributed the measured increase in impulse primarily due to the partial fill effect.

Additional studies[11,12] have investigated the effect of ejectors on performance. Allgood and Gutmark[11]

carried out two-dimensional, reactive numerical calculations of ejectors on detonation tubes predicting the thrust as a function of the ejector dimensions. Allgood et al.[12] carried out an experimental study using a high-speed shadowgraph imaging system to visualize the flow from their two-dimensional ejector. No experimental thrust measurements were obtained for the different ejector configurations in the later work of Allgood et al.[12] Ejectors are designed to entrain additional environment air into the flow to increase the exhaust gas momentum and the thrust. While the use of ejectors attached to the end of detonation tubes is an interesting problem, it is beyond the scope of this work.

The behavior of detonations propagating through variable area geometries has also been investigated. In particular, Tzuk et al.[13] and Grigor'ev[14] have experimentally studied the expansion of detonation products through diverging nozzles that were seeded with particles in order to visualize the flow. They both observed an increase in particle velocities as the flow expanded through the diverging nozzle. As in our experiments, the combustible mixture in their experiments did not fill the nozzle, however they did not measure thrust. An experimental study carried out by Thomas and Williams[15] investigated the behavior of a detonation wave in two-dimensional curved channels and diverging nozzles. The channels and nozzles were completely filled with the combustible mixture and sooted foils were used to record the detonation behavior as the geometry changed. Akbar et al.[16] studied the propagation of detonations through converging channels and extended Whitham's method of shock dynamics to the detonation case in order to design the channel. In the work of Thomas and Williams[15] and Akbar et al.,[16] there was no effort to measure impulse.

While the studies of Cambier and Tegner,[3] Eidelman and Yang,[4] Yang et al.,[5] Guzik et al.,[6] Morris,[8] Cooper et al.,[9] and Falempin et al.[10] have studied nozzles on detonation tubes, this experimental data systematically investigates the effect of nozzles on impulse under varying environment pressures. With the nozzles tested here, the effect of divergence angle, volumetric fill fraction, and nozzle length are investigated.

## II. Experiments

### A. Detonation tube

The detonation tube is a smooth-walled cylinder made of 6061-T6 aluminum that is 1.014 m in length, has an inner diameter of 76.2 mm, and a wall thickness of 12.7 mm. One end of the tube is sealed with a plate called the "thrust surface" and contains the spark plug, a pressure transducer, and a gas-inlet fitting. The other end of the tube is open, but is initially sealed with a Mylar diaphragm to contain the combustible mixture prior to ignition. In addition to the pressure transducer mounted in the thrust surface, two more pressure transducers located 0.58 m and 0.99 m from the thrust surface and ten ionization gauges (spaced 10.4 cm apart) were installed to measure wave arrival times.

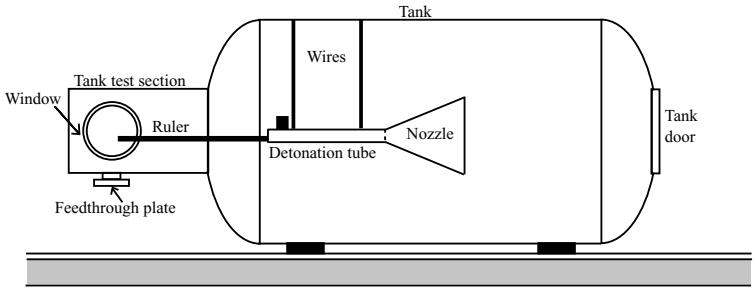


**Figure 1. Schematic of experimental facility.**

### B. Large tank

The single-cycle impulse measurements were carried out by sealing the detonation tube within a large tank that is actually the test section and dump tank of Caltech's T5 Hypersonic Wind Tunnel facility (Fig. 1). The volume internal to the tank but external to the detonation tube is the "environment" and is air at pressure $P_0$ while the initial pressure of the combustible mixture is at pressure $P_1$. The environment pressure could

be varied between 100 and 1.4 kPa, thus extending the capabilities of the ballistic pendulum method to obtain accurate single-cycle impulse measurements at a variety of operating conditions.

The tank has an internal volume of approximately 12,500 L and is roughly the shape of a horizontal cylinder with an inner diameter of 2 m and a length of 4 m. The attached test section (labeled in Fig. 1) is a cylinder approximately 0.7 m in diameter and 1.3 m in length. It contained two windows on each side through which the tube's motion was observed. A ruler extending off the front of the detonation tube and into view of the test section windows was filmed by a digital camera situated outside the tank. From this recording of the tube's periodic motion, the maximum deflection was converted into impulse. A door on the end of the tank downstream of the detonation tube exhaust was used for access inside the tank to install a new diaphragm between each experiment.

### C. Extensions

The exit condition of the detonation tube was modified by attaching a nozzle onto the open end of the tube. The diaphragm was positioned between the exit plane of the tube and the inlet to the nozzle so that the nozzle contained air at the environment conditions. Descriptions of the extensions follow.

*Diverging nozzles*

Three conical diverging nozzles (Fig. 2) were constructed from a rolled piece of 6061-T6 aluminum sheet with a thickness of 0.16 cm. The corresponding dimensions for each nozzle appear in Table 1. A fourth "diverging" nozzle had a 0° half angle and is also referred to as a straight extension.

| Description | Length (m) | $\phi$ (°) | $D_{inlet}$ (mm) | $D_{exit}$ (mm) | $A_{exit}/A_{inlet}$ |
|---|---|---|---|---|---|
| 0°-0.6 m | 0.6 | 0 | 76.2 | 76.2 | 1 |
| 8°-0.3 m | 0.3 | 8 | 63.5 | 152.0 | 5.7 |
| 12°-0.3 m | 0.3 | 12 | 76.2 | 194.0 | 6.5 |
| 12°-0.6 m | 0.6 | 12 | 76.2 | 311.0 | 16.7 |

**Table 1. Dimensions of the diverging nozzles.**

(a) (b)

**Figure 2. Photographs of the three diverging nozzles; (a) left: 12° - 0.3 m, right: 8° - 0.3 m; (b) left: 12° - 0.3 m, right: 12° - 0.6 m**

*Converging-diverging nozzles*

The effect of a throat restriction upstream of a diverging nozzle was tested by attaching a separate throat section onto the diverging nozzles with a 12° half angle. Each throat section had an inlet area equal to the detonation tube cross-sectional area, followed by a decrease in area to the throat. After the throat, the area increased until it equaled the tube cross-sectional area (also equal to the inlet area of the diverging nozzles). This created a single converging-diverging nozzle that had a continuous increase in area from the throat to the nozzle exit. An illustration of the general shape of the converging-diverging throat section appears in Fig. 3 and the exact dimensions are tabulated in Table 2.

The converging part of the throat had a 45° half angle while the half angle after the throat was 12° to match the diverging nozzles. Three different converging-diverging sections were installed on the two diverging nozzles with a 12° half angle for a total of six test configurations. Because the inlet and exit half angles of the converging-diverging section were fixed, the length of each fixture varied in order to obtain the desired throat area. Thus, the section with the smallest throat area had the longest length as illustrated in Table 2.

| Description | Length (mm) | $D_{throat}$ (mm) | $A_{throat}/A_{inlet}$ |
|---|---|---|---|
| CD-0.75 | 29.0 | 66.0 | 0.75 |
| CD-0.54 | 57.9 | 55.9 | 0.54 |
| CD-0.36 | 86.9 | 45.7 | 0.36 |

**Table 2. Dimensions of the converging-diverging throat sections. Refer to Fig. 3 for the corresponding labels.**

## III. Experimental data

Each nozzle was attached to the detonation tube and the impulse was measured as the environment pressure varied between 100 and 1.4 kPa. The combustible mixture was stoichiometric ethylene-oxygen at an initial pressure of 80 kPa and a diaphragm thickness of 105 $\mu$m was used to ensure experimental repeatability at low environment pressures. Over the range of tested environment pressures, the addition of a diverging nozzle always increased the specific impulse over the case of a plain tube. The addition of a converging-diverging nozzle generally reduced the impulse except at the lowest values of $P_0$. The effect of each nozzle on the impulse is discussed in the following sections.

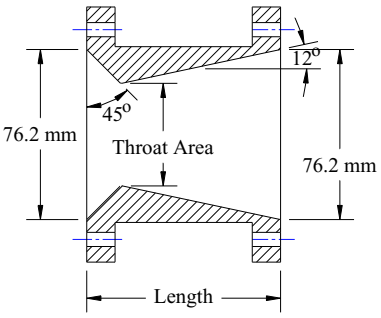


**Figure 3. Illustration of converging-diverging throat section. See Table 2 for the exact dimensions.**

*0°-0.6 m nozzle*

The impulse obtained with the straight extension (characterized as a diverging nozzle with a 0° half angle) is plotted as a function of the environment pressure in Fig. 4. At 100 kPa, the largest increase in specific impulse, equal to 26%, over the plain tube case is observed. This can be attributed to the partial fill effect provided by the tamper mass. As the environment pressure decreases, a corresponding decrease in the tamper mass results and the impulse decreases as predicted by the partial fill model. For the lowest environment pressure, $P_0 = 1.4$ kPa, the tamper mass has gone to zero. In this case, the increase in impulse does not go to zero as predicted by the partial fill model, but instead increases by 13% over the case of a plain tube since the extension acts to confine the exhaust flow and slow the rate of pressure decrease at the thrust surface.

*8°-0.3 m nozzle*

The impulse obtained with the 8°-0.3 m diverging nozzle is plotted as a function of the environment pressure in Fig. 5. Although this nozzle has half the length of the straight extension, the explosive mass fractions are approximately equal (0.61 for 8°-0.3 m and 0.58 for 0°-0.6 m) at an environment pressure of 100 kPa. While the partial fill model predicts that the same impulse should result from the two nozzles, only a 6.4% increase in impulse is observed with the 8°-0.3 m nozzle whereas the straight extension observed a 26% increase. This illustrates that the partial fill effect is more efficient at increasing the impulse in one-dimensional geometries than two-dimensional geometries. Unlike the straight extension, the impulse of the 8°-0.3 m nozzle increases as $P_0$ decreases. At $P_0 = 1.4$ kPa, the impulse increases 29% over the plain tube and 16% over the straight extension.

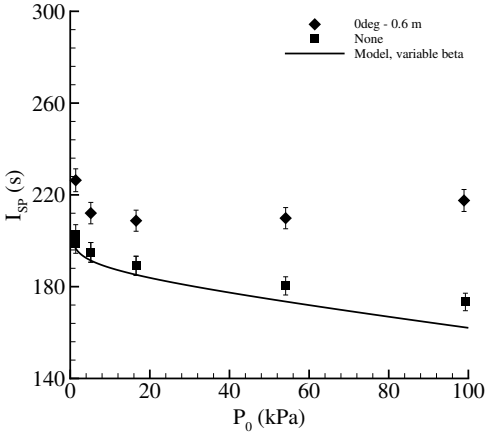


**Figure 4. $I_{sp}$ versus $P_0$ for the 0°-0.6 m nozzle and no nozzle. The modified impulse model (Eq. 1) is also plotted.**

*12°-0.3 m nozzle*

The impulse obtained with the 12°-0.3 m diverging nozzle is plotted as a function of the environment pressure in Fig. 6. The impulse with the 12°-0.3 m nozzle remains constant as the environment pressure decreases from 100 kPa to 54 kPa. As previously observed with the straight extension, the impulse is affected by the tamper mass contained in the nozzle. As the environment pressure decreases, the tamper mass $N$ decreases and does so at a faster rate the larger the nozzle volume $\Delta N = \Delta P_0 V/RT_0$. Thus, for a given decrease in the environment pressure $P_0$, the change in the tamper mass is greater for the larger nozzle volume. When the environment pressure has decreased sufficiently and the tamper is small, quasi-steady flow exists in the nozzle. It is the competition between these two effects that ultimately determine the impulse. In the case of the 12°-0.3 m nozzle, as the environment pressure decreases from 100 kPa to 54 kPa these two effects are balanced and no net change in the measured specific impulse is observed.

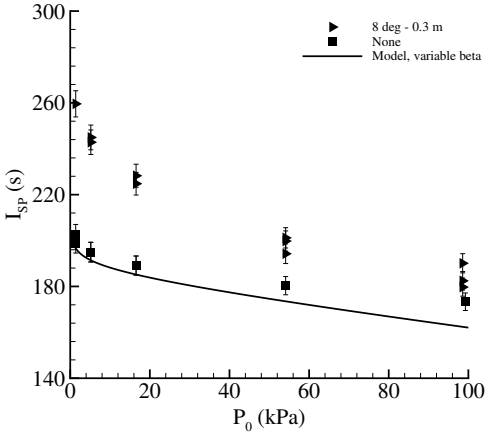


**Figure 5. $I_{sp}$ versus $P_0$ for the 8°-0.3 m nozzle and no nozzle. The modified impulse model (Eq. 1) is also plotted.**

As the environment pressure decreases below 54 kPa, the tamper mass is sufficiently low and the effect of quasi-steady flow within the nozzle acts to increase in the impulse over the case of the plain tube. At the lowest environment pressure of $P_0 = 1.4$ kPa, the 12° half angle nozzle generates more impulse (a 36% increase over the plain tube case) than the smaller nozzle with an 8° half angle and the same length.

*12°-0.6 m nozzle*

The impulses obtained with the 12°-0.6 m diverging nozzle are plotted as a function of the environment pressure in Fig. 7. The 12°-0.6m nozzle has the largest volume of all the nozzles tested and also generates the largest increases in impulse. At an environment pressure of 100 kPa, a 72% increase in impulse is observed and this is due to the large tamper mass contained in the nozzle. As $P_0$ decreases, the tamping action of the nozzle gas decreases and the impulse decreases. This was observed previously with the 0°-0.6 m nozzle

and the shorter 12° half angle nozzle. However, a smaller change in impulse was observed in response to a change in the environment pressure as compared to the 12°-0.6m nozzle because of their smaller volumes. When the environment pressure reaches approximately 10 kPa, the impulse is observed to reach a minimum. At this point the tamper mass is sufficiently small such that the partial fill effect is negligible. The nozzle expands the flow and the walls of the nozzle experience a positive pressure difference which also contributes to increase the impulse. For environment pressures less than 10 kPa, the impulse increases with decreasing environment pressure. As expected, the shorter 12° half angle nozzle expands the flow less than the longer one does. Note that the maximum increase in impulse due to flow expansion at the lowest $P_0$ is less than the increase in impulse due to the partial fill effect at $P_0 = 100$ kPa. This is likely due to significant flow separation from the nozzle walls at $P_0 = 100$ kPa and is discussed in §IV.D.

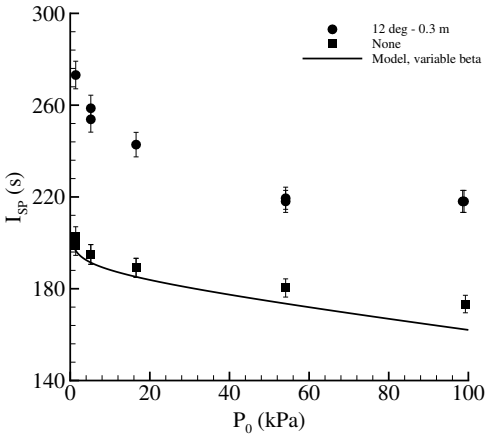


**Figure 6. $I_{sp}$ versus $P_0$ for the 12°-0.3 m nozzle and no nozzle. The modified impulse model (Eq. 1) is also plotted.**

### A. Converging-diverging nozzles

The two diverging nozzles with a 12° half angle were tested with the three converging-diverging sections. The experimental data appears in Fig. 8(a) for the 0.3 m nozzle and in Fig. 8(b) for the 0.6 m nozzle as a function of the environment pressure. Analyzing the control volume shown in Fig. 9 for the case with a converging-diverging nozzle requires consideration of the nozzle surfaces that have $x$-direction components such as the thrust surface $A_{TS}$, the converging portion of the nozzle $A_C$, and the diverging portion of the nozzle $A_D$.

The total force on the tube depends not only on the time-varying pressure on the thrust surface, but also the time-varying pressure on these additional areas.

$$I = \iint_{A_{TS}} [P_{TS}(t) - P_0]\hat{x} \cdot \hat{n}\ dAdt + \iint_{A_C} [P_0 - P_C(t)]\hat{x} \cdot \hat{n}\ dAdt + \iint_{A_D} [P_D(t) - P_0]\hat{x} \cdot \hat{n}\ dAdt \quad (2)$$

Where pressure $P_C$ acts on area $A_C$, pressure $P_D$ acts on area $A_D$, $\hat{n}$ is a unit vector normal to each surface, $\hat{x}$ is a unit vector aligned with the $x$-axis which is the desired direction of motion.

The relative size of these three force contributions determines the impulse. When the environment pressure is large, the impulse decreases as the throat area decreases. This can be attributed to the presence of large regions of separated flow in the diverging portion of the nozzle and so the contribution of the third term in Eq. 2 is small. The second term is negative and increases in absolute magnitude as the throat becomes smaller resulting in a net decrease in impulse. For the nozzle with a length of 0.3 m, a maximum loss impulse of 27% was observed with the most restrictive converging-diverging section whereas a 42% loss in impulse was observed for the 0.6 m long nozzle. Estimating the loss in impulse by decreasing the throat area by 36% (as is the case for the data of CD-0.36 in

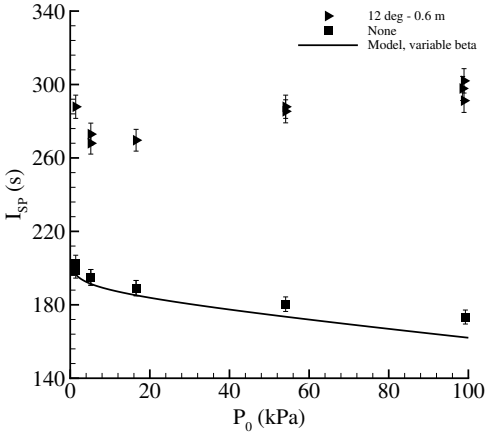


**Figure 7. $I_{sp}$ versus $P_0$ for the 12°-0.6 m nozzle and no nozzle. The modified impulse model (Eq. 1) is also plotted.**

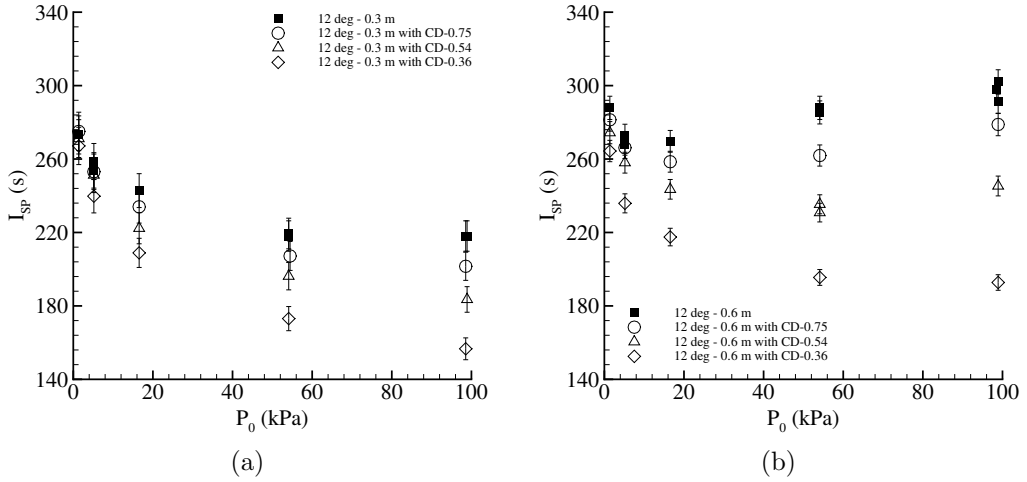


**Figure 8. Specific impulse data for the 12° half angle nozzles that are (a) 0.3 m long and (b) 0.6 m long with converging-diverging sections as a function of the environment pressure.**

Fig. 8) results in a 36% loss in impulse if the impulse model is used $I = KV/U_{CU}(P_3 - P_0)$ where $V = AL$ and the state 3 pressure is assumed to equal the pressure on the convergent portion of the nozzle $A_C$.

As the environment pressure decreases, the effect of the converging-diverging restrictions decreases such that at $P_0 = 1.4$ kPa, each nozzle configuration gives approximately the same value of impulse. In this situation, the large pressure ratio across the nozzle dominates the impulse. While the second term of Eq. 2 acts to decrease the impulse, the flow expansion and a positive pressure differential across the diverging nozzle walls is significantly greater and the third term of Eq. 2 acts to increase the impulse. Sample thrust surface pressure histories are presented in Fig. 10 for the 12°-0.3 m nozzle with the most and least restrictive converging-diverging sections and environment pressures of (a) 100 kPa and (b) 1.4 kPa. Multiple wave reflections are observed for the most restrictive converging-diverging section.

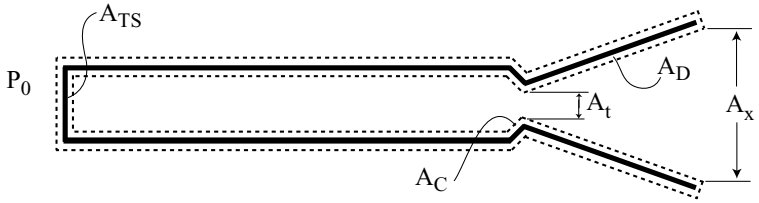


**Figure 9. Control volume for a tube with a converging-diverging nozzle.**

## B. Comparisons

The diverging nozzles with the 8° and 12° half angles are plotted together in Fig. 11(a) illustrating the effect of the half angle (compare data for the 8°-0.3 m and 12°-0.3 m nozzles) and the effect of nozzle length (compare data for the 12°-0.3 m and 12°-0.6 m nozzles). The partial fill effect has been previously observed for the different nozzles as the environment pressure decreases from 100 kPa. The nozzle with the largest volume generates the largest increases in impulse over the baseline case of a plain tube. As previously observed, the nozzle dimensions also affect how quickly the impulse decreases as the environment pressure decreases. For example, the impulse from the 12°-0.6 m with the largest volume experiences the largest decrease in impulse as compared to the other diverging nozzles when the environment pressure decreases

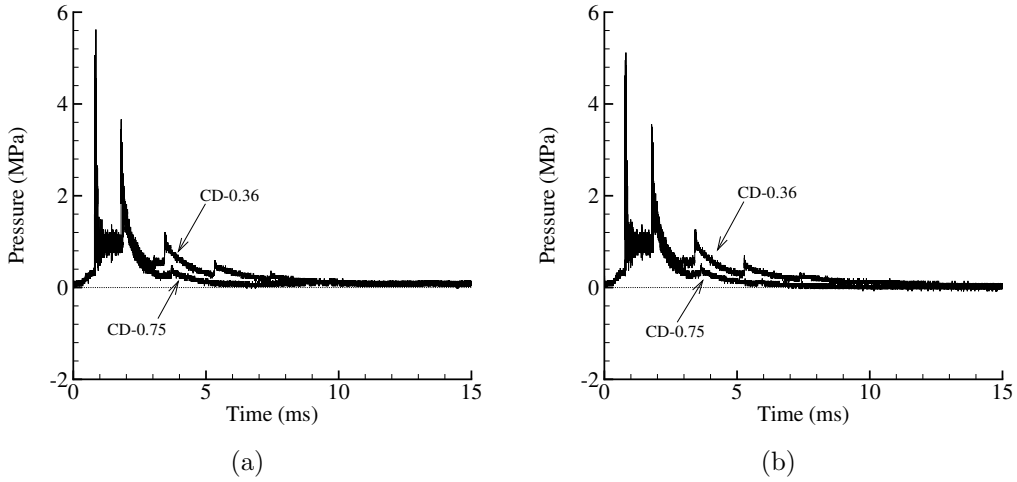


**Figure 10. Specific impulse data for the 12°-0.3 m nozzles with converging-diverging sections for environment pressures of (a) 100 kPa and (b) 1.4 kPa.**

from 100 to 54.5 kPa. The impulse from the 12°-0.3 nozzle which has the second largest volume is actually observed to remain constant as the environment pressure decreases from 100 to 54.5. The impulse from the 8°-0.3m nozzle which has the smallest volume of the diverging nozzles is just observed to increase as the environment pressure decreases. In this case, the increase in impulse due to the increased pressure differential across the thrust surface is sufficiently large enough to exceed the decrease in impulse caused by a reduction in the tamper mass as the environment pressure decreases from 100 to 54.5 kPa.

For each diverging nozzle there is an environment pressure where neither the tamper mass or the flow expansion of the nozzle dominate the impulse. This point is observed most clearly for the large 12°-0.6m nozzle between environment pressures of 16.5 and 5.2. For the shorter 12°-0.3m nozzle this occurs between 100 and 54.5 kPa. This point is not observed for the 8°-0.3m nozzle as the expansion by the nozzle seems to always dominate the impulse.

Comparison of the 8°-0.3m nozzle and the straight extension clearly show the effect of these competing processes for two nozzles with the same volume. Their impulse data are plotted in Fig. 11(b). These two nozzles have approximately the same explosive mass fraction at $P_0 = 100$ kPa, yet the straight extension generates a higher impulse. As $P_0$ decreases and the tamper mass goes to zero, the diverging nozzle generates higher values of impulse due to the flow expansion provided by the divergent shape.

## IV. Data analysis assuming quasi-steady nozzle flow

The experimental impulse data suggest that quasi-steady flow expansion occurs within the nozzles at the lower environment pressures where the partial fill effects and tamper mass are negligible (Fig. 11). From this observation and the lack of other analysis methods for detonation tube nozzles, we analyze the measured impulse data assuming that quasi-steady nozzle flow is established. For this analysis to be reasonable, several crucial assumptions are required.

First, it is assumed that quasi-steady flow through the nozzle is present for a majority of the blowdown process. This implies a rapid startup time and a delayed time of unchoking at the nozzle inlet. The startup time is defined as the time between when the transmitted shock enters the nozzle inlet until the establishment of quasi-steady flow and is known[17,18] to depend primarily on the initial nozzle pressure ratio. At large values of $P_0$ where the pressure ratio $P_3/P_0$ is small, the establishment of quasi-steady nozzle flow is not expected to

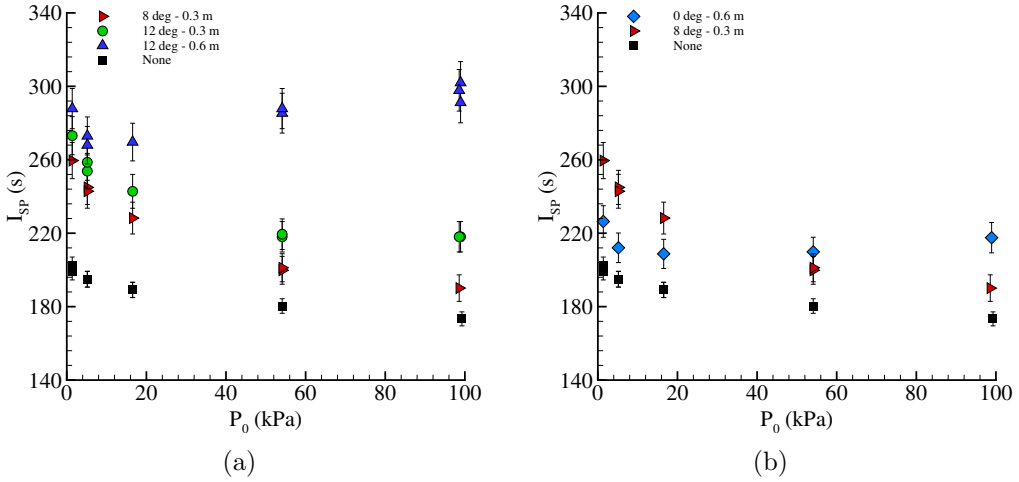


**Figure 11. Specific impulse as a function of environment pressure for detonation tubes with (a) diverging nozzles and (b) the straight extension and the 8°-0.3 m nozzle.**

occur. However, at the lowest values of $P_0$ and larger values of $P_3/P_0$, rapid startup followed by quasi-steady flow is expected.

Second, it is assumed that the pressure decrease upstream of the nozzle inlet does not significantly affect the quasi-steady nozzle flow and can be modeled. In devices with steady combustion processes, the nozzle inlet conditions are constant in time. In a detonation tube, the unsteady processes of detonation propagation and the subsequent unsteady blowdown to ambient pressure generate unsteady nozzle inlet conditions.

If these effects are assumed to be minor or can be reasonably modeled, then the impulse from a detonation tube with a nozzle can be compared to the impulse from an ideal, steady flow nozzle with the same dimensions. In the case of a steady flow nozzle that is pressure-matched to the environment, the exhaust gas velocity at the nozzle exit plane determines the specific impulse and the total force on the engine equals $\dot{m}u_x$.

$$I_{sp} = \frac{I}{\int_0^t \dot{m}gdt} = \frac{\int_0^t \dot{m}u_x dt}{\int_0^t \dot{m}gdt} = \frac{u_x}{g} \tag{3}$$

This force is determined by drawing a control volume around the device (Fig. 12) and recognizing that the mass flow of the exhaust $\dot{m}$ is constant in time.

When this same control volume is applied to a detonation tube, the unsteadiness of the flow must be considered. The general unsteady mass conservation for the control volume is

$$\frac{d\mathcal{M}}{dt} + \dot{m}(t) = 0 \tag{4}$$

The general unsteady momentum conservation for the control volume consists of the pressure forces and the exhaust gas momentum.

$$F(t) = \dot{m}(t)u_x(t) + A_x[P_x(t) - P_0] + \frac{d}{dt}\int_V \rho u dV \tag{5}$$

When the nozzle inlet flow is choked, the mass flow rate depends on the throat area, the upstream pressure, and the upstream product gas state $T_i/\mathcal{W}$. Because the detonation tube pressure decreases through the blowdown process, the mass flow rate will also decrease. For pressure-matched nozzle exit conditions, the

middle term of Eq. 5 equals zero. The last term corresponds to the unsteady variation of momentum inside the control volume. This term is typically considered to be zero in steady flow devices where the combustion chamber cross section is large compared to the nozzle section and the nozzle approach velocity is typically small so the change in momentum due to this increase in velocity can be neglected.[19] In the case of a detonation tube, not only is the tube cross section equal to the nozzle inlet cross section but the unsteady waves inside the tube alter the gas momentum over time. The detonation wave increases the gas momentum which is subsequently decreased by expansion through the Taylor wave. Particles at state 3 behind the Taylor wave have zero velocity and so their unsteady variation of momentum is zero. Their momentum increases after they pass through the wave reflected from the open tube end which accelerates them away from the thrust surface and out of the tube. Thus, the third term of Eq. 5 is expected to be positive when considering a detonation tube, but for the later purpose of using the analysis techniques of steady nozzle flows, this term is assumed to be small and can be neglected.

As discussed, the assumptions that have been made are numerous but necessary in order to use the standard equations of ideal, steady flow to analyze the experimental data for detonation tubes with nozzles. To do so, the experimental specific impulse data are converted with Eq. 3 into an average exhaust velocity $\overline{u_x}$ that is comparable to the constant exhaust velocity $u_x$ of a steady flow device. The merit of conducting this analysis is to generate an ultimate measure of performance for detonation tubes with nozzles. Analysis methods that consider all the unsteadiness of the device would require detailed numerical calculations for each specific configuration. Therefore, steady flow through the nozzle is presently assumed and the methods of calculation appear in the next section. Non-ideal processes including changing nozzle inlet conditions, boundary layer separation, partial fill effects, and transient flow that can be modeled or estimated are discussed in more detail in later sections.

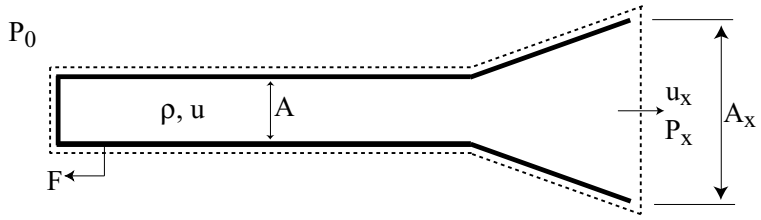


**Figure 12. Control volume surrounding engine.**

### A. Steady flow nozzle calculations

The inlet state to the detonation tube nozzle must be carefully chosen to facilitate an appropriate comparison between the average exhaust gas velocity $\overline{u_x}$ and the predicted steady exhaust gas velocity $u_x$. This choice is complicated by the unsteady wave processes propagating through the detonation tube. For a finite length tube, a reflected expansion wave that propagates through the products towards the thrust surface is generated once the detonation wave reaches the open end of the tube. This unsteady expansion accelerates the flow from zero velocity at state 3 to a nonzero velocity out of the tube. For a tube without a nozzle, the flow is accelerated to sonic conditions at the open end. When a nozzle is attached, sonic conditions are assumed to exist at the nozzle inlet. The flow velocity at this sonic point is calculated assuming the flow steadily and adiabatically expands from state 3 to sonic conditions such that the total enthalpy remains constant and equal to the enthalpy at state 3.

$$u(P) = \sqrt{2[h_3 - h(P)]} \tag{6}$$

From the sonic point at the nozzle inlet, the flow is steadily expanded and the thermodynamic states throughout the nozzle can be calculated in three ways. First, the extreme assumptions of either equilibrium or frozen flow can be made and thermodynamic computations carried out to obtain the enthalpy as a function of pressure on the isentrope. Second, elementary perfect gas relationships can be used to get analytic formulas

for exhaust velocity as a function of pressure. Third, steady flow simulations with a detailed chemical reaction mechanism for specific nozzle geometries can be carried out to find exit conditions and specific impulses.

With the extreme assumptions of either equilibrium or frozen composition, the nozzle flow is calculated using STANJAN.[20] The results of flow velocity as a function of pressure are plotted in Fig. 13(a) starting from state 3 ($P_3 = 970$ kPa for $C_2H_4$-$O_2$ at $P_1 = 80$ kPa), expanding to the sonic point, and then through the nozzle.

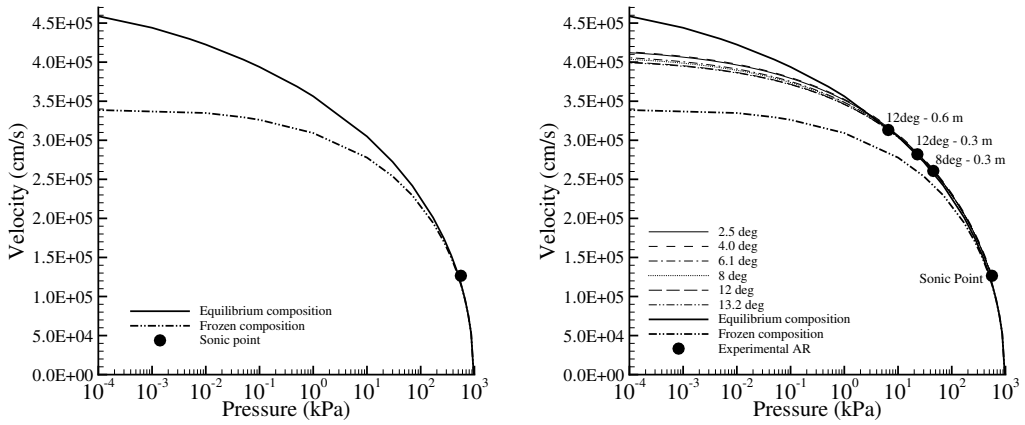


**Figure 13. (a) Acceleration of flow from state 3 through the sonic point and subsequent nozzle assuming either equilibrium or frozen composition. (b) Comparison of flow velocity considering finite rate kinetics compared to thermodynamic calculations considering equilibrium and frozen composition as a function of pressure.**

A limiting velocity and specific impulse is predicted by expansion to low pressures.

$$u \rightarrow u_{max} = \lim_{P \rightarrow 0} \sqrt{2[h_t - h(P)]} \tag{7}$$

In general, since $h = h(\mathbf{Y}, T)$, species and temperature variations must be related to the pressure variation in order to predict $h$.

The second method for calculating the nozzle flow is with the perfect gas relationships (Eq. 8).

$$u_x = \sqrt{\frac{2\gamma}{\gamma - 1} RT_i \left[ 1 - \left( \frac{P_x}{P_i} \right)^{(\gamma-1)/\gamma} \right] + u_i^2} \tag{8}$$

Equation 8 can be solved for any known inlet conditions $P_i, u_i, \gamma, T_i/\mathcal{W}$. The corresponding temperature at any state is determined from the isentropic relation $T \sim P^{(\gamma-1)/\gamma}$ and the area is determined from the mass equation $d(\rho u A) = 0$. However, Eq. 8 uses a constant value of $\gamma$ and product gas molecular weight, so the effect of species variation within the expansion is not considered.

Finally, the third method for calculating nozzle flows utilizes detailed chemical reaction mechanisms and finite rate kinetics. In the case of steady supersonic flow through rapidly diverging nozzles, the effects of finite rate kinetics can significantly affect the exit state and therefore, the measured impulse.[21] To evaluate the extent of chemical kinetics on the impulse from detonation tube nozzles with dimensions similar to these experiments, the steady flow conservation equations in one-dimension with the species equation are solved.

$$\frac{d}{dx} (\rho u A) = 0 \tag{9}$$

$$\rho u \frac{du}{dx} + \frac{dP}{dx} = 0 \tag{10}$$

$$\frac{d}{dx}\left(h + \frac{u^2}{2}\right) = 0 \tag{11}$$

$$u \frac{d\mathbf{Y}}{dx} = \mathbf{\Omega} \tag{12}$$

For an adiabatic change, the energy equation can be written in terms of the thermicity.

$$\frac{dP}{dt} = c^2 \frac{d\rho}{dt} + \rho c^2 \dot{\sigma} \tag{13}$$

The thermicity term $\dot{\sigma}$ corresponds to the pressure change due to chemical reaction and $c$ is the frozen sound speed. In the absence of chemical reaction, Eq. 13 reduces to $dP = c^2 d\rho$, the usual relationship for nonreactive isentropic flow.

Equation 13 is substituted into Eqs. 9-12 and the derivatives with respect to position are converted into derivatives with respect to time with the transformation $dt = dx/u$ (Eqs. 14-17). This means that a single particle is tracked, recording its state as a function of time. Since the flow field is steady, all particles have the same history.

$$\frac{dP}{dt} = \frac{\rho u^2}{1 - M^2}\left(\frac{u}{A}\frac{dA}{dx} - \dot{\sigma}\right) \tag{14}$$

$$\frac{d\rho}{dt} = \frac{\rho}{1 - M^2}\left(M^2 \frac{u}{A}\frac{dA}{dx} - \dot{\sigma}\right) \tag{15}$$

$$\frac{d\mathbf{Y}}{dt} = \mathbf{\Omega} \tag{16}$$

$$\frac{dx}{dt} = u \tag{17}$$

The Mach number $M$ equals $u/c$. The area terms are solved from the prescribed nozzle shape $A_N$ normalized by the throat area which equals the tube cross-section $A$ for the diverging nozzles.

$$\frac{A_N(x)}{A} = \left(1 + \frac{x \tan(\alpha)}{R_0}\right)^2 \tag{18}$$

The equations 14-18 are simultaneously integrated and the GRI3Mech mechanism is used to obtain real gas enthalpies and reaction rates. A series of computations with different nozzle half angles between 2.5° and 13.2° were carried out in ethylene-oxygen mixtures with 80 kPa initial pressure. The starting condition for the calculation is the state parameters and species amounts at the sonic point (Fig. 13a). The resulting gas velocity through the nozzle as the pressure decreases is plotted in Fig. 13(b) for the different half angles along with the equilibrium and frozen composition results of Fig. 13(a).

The flow expansion considering finite rate chemical kinetics is represented by the equilibrium predictions until the pressure has decreased to approximately 10 kPa. At this point, the flow velocity calculated with finite rate kinetics is greater than the velocity predicted assuming frozen composition but less than the velocity predicted assuming equilibrium composition. Investigation of the species mole fractions as a function of pressure identify that the mole fractions of $H_2O$ stop changing once the pressure reaches approximately 10 kPa (Fig. 14) and the mole fractions of $CO_2$ stop changing once the pressure reaches approximately 1 kPa (Fig. 15). As the pressure continues to decrease, these species amounts are frozen at values between 0.32 and 0.34 for $H_2O$ and 0.25 and 0.30 for $CO_2$ depending on the nozzle half angle.

At equilibrium, the mole fractions for both $H_2O$ and $CO_2$ should approach 0.5 as specified by the stoichiometric reaction, $C_2H_4 + 3O_2 \rightarrow 2H_2O + 2CO_2$, but this is not the case when the finite chemical reaction rates are considered. The nozzle with the smallest half angle of 2.5° yields the highest mole fractions for $H_2O$ and $CO_2$ due to the slower rate of pressure decrease (Fig. 16) unlike that of the nozzle with a large half angle. As the flow expands, the recombination and dissociation reactions are important. The recombination reactions release energy into the flow, elevating the temperature and pressure over the case with no chemical reaction. This recombination results in an increase in the amounts of $H_2O$ and $CO_2$ and a decrease in the amount of OH and CO. Additional atoms are found to be in smaller amounts in the O, H, and $O_2$ species.

Also plotted on Fig. 13(b) are points corresponding to the area ratios of the experimental nozzles. These points indicate the predicted exit pressure and velocity of the product gases assuming steady expansion and pressure matched conditions. Their locations on the velocity-pressure curve indicate that, in the present experiments, the products are in equilibrium throughout the entire expansion process.

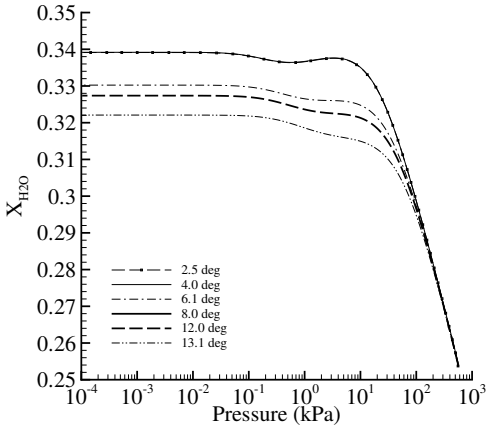


**Figure 14. Mole fractions of $H_2O$ molecules as a function of pressure for different diverging nozzles.**

The experimental values of $\overline{u_x}$ are plotted in Fig. 17(a) with the steady flow predictions of velocity as a function of pressure. The experimental values of $\overline{u_x}$ are observed to increase with decreasing environment pressure as do the steady flow predictions. However, the experimental values are lower than the steady predictions due to the unsteadiness of the flow and the fact that the exhaust gases are not pressure-matched to the environment pressure during the entire blowdown event as is assumed by using Eq. 3. The next sections discuss in more detail some of the non-ideal effects present in detonation tube nozzles.

## B. Changing nozzle inlet state

In a detonation tube, the nozzle inlet state previously based on state 3 is not constant in time. After the first characteristic of the Taylor wave reflects off the open tube end and reaches the thrust surface, the pressure is decreasing at all locations within the tube implying that it is not reasonable to assume a constant nozzle inlet state that is based on state 3. A better choice from which to start the expansion to the sonic point is from an intermediate pressure that represents the average pressure within the tube over the entire cycle. This supports the findings of Harris et al.[7] who specify that the average detonation tube pressure determines the impulse and should be maximized. Averaging the experimental pressure traces obtained for mixtures with an initial pressure of 80 kPa yields an intermediate value of 400 kPa. Starting the expansion with this average value of pressure results in better agreement between the steady flow predictions experimental data (Fig. 17b).

Here it is significant to note that several of the data points, in particular those for the 12°-0.6m nozzle and pressures greater than 10 kPa and those for the 12°-0.3m nozzle and pressures greater than 50 kPa, do not follow the trend of

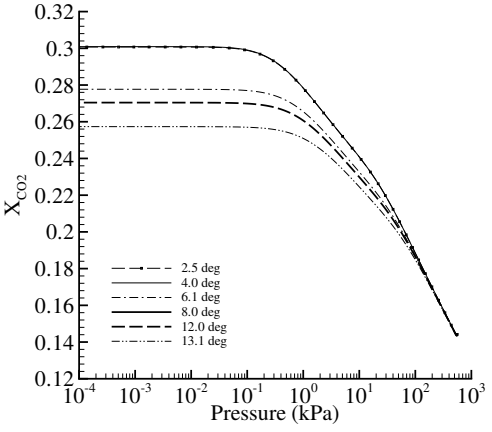


**Figure 15. Mole fractions of $CO_2$ molecules as a function of pressure for different diverging nozzles.**

the other data for the same nozzle. For these data points, the tamper mass of the nozzle is large enough such that the partial fill effect dominates the impulse.

### C. Partial fill effects

The impulse data is plotted in Fig. 18 as a function of the explosive mass fraction for each nozzle and environment pressure along with the Gurney model of partial filling (refer to Cooper[2] for the model derivation for partially filled detonation tubes). The experimental data is normalized by $I^{\circ}_{sp} = 173$ s which is the experimentally measured value from a fully filled tube without a nozzle and a 105 $\mu$m thick diaphragm in ethylene-oxygen mixtures at an initial pressure of 80 kPa.

The experimental data of Fig. 18 can be divided into three groups. The first group has mass fractions less than 0.4. This data corresponds to the highest environment pressure and the largest nozzle. Since the partial fill model is based on one-dimensional geometries it overpredicts the impulse obtained from tubes with diverging nozzles. Thus, when the partial fill effect of the tamper dominate the impulse, a larger increase in impulse is gained with a straight extension rather than a diverging nozzle. For these cases of large nozzles and high environment pressures, the partial fill effect is of greatest importance. This effect lessens as the environment pressure decreases and the explosive mass fraction increases.

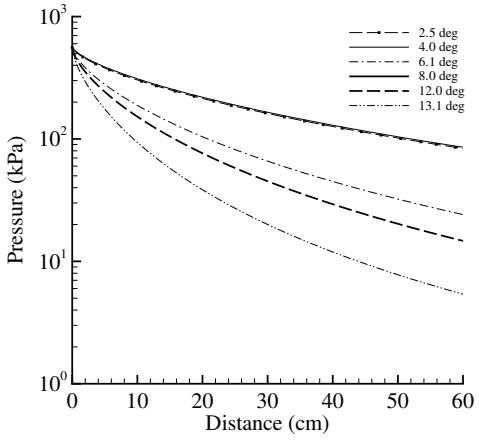


**Figure 16. Pressure as a function of distance from the nozzle throat for different half angles assuming finite reaction rates.**

For intermediate mass fractions between 0.4 and 0.75, the partial fill model is in reasonable agreement with the data. This data corresponds to the larger environment pressures and the nozzles with the smallest volumes where the effect of the divergent shape is minimized. The data of the straight extension at the larger environment pressures is observed to be best predicted by the partial fill model for this range of explosive mass fractions.

The data at the highest mass fractions, greater than 0.75, correspond to all of the nozzles and the lowest environment pressures. It is obvious that the experimental results are uncorrelated with the explosive mass fraction for this situation. In this regime, quasi-steady flow is important and the previous steady flow analysis applies. The partial fill model is not able to model the increased blowdown time and flow expansion that occurs within the nozzle.

### D. Boundary layer separation

Sutton[19] states that a rough criterion for jet separation is when the nozzle exit pressure is less than or equal to 0.4 times the environment pressure. In other words, as long as the nozzles exhaust at a pressure that is greater than $0.4 \times P_0$, then flow separation of the boundary layer from the nozzle walls is not expected. Sutton[19] states that other factors such as the pressure gradient, nozzle contour, boundary layer, and flow stability affect separation in addition to the nozzle exit pressure and the environment pressure.

Due to the dearth of research on detonation tube nozzle flow this general relationship for flow separation must suffice. An estimation of the nozzle exit pressure corresponding to each experimental area ratio is obtained from the previous steady flow predictions with finite rate kinetics based on an average tube pressure for the nozzle inlet condition. The pressure decrease through the nozzle is plotted in Fig. 19 along with points corresponding to the area ratios of the experimental nozzles. The separation criteria for each of the experimentally tested environment pressures between 100 kPa and 1.4 kPa are also indicated.

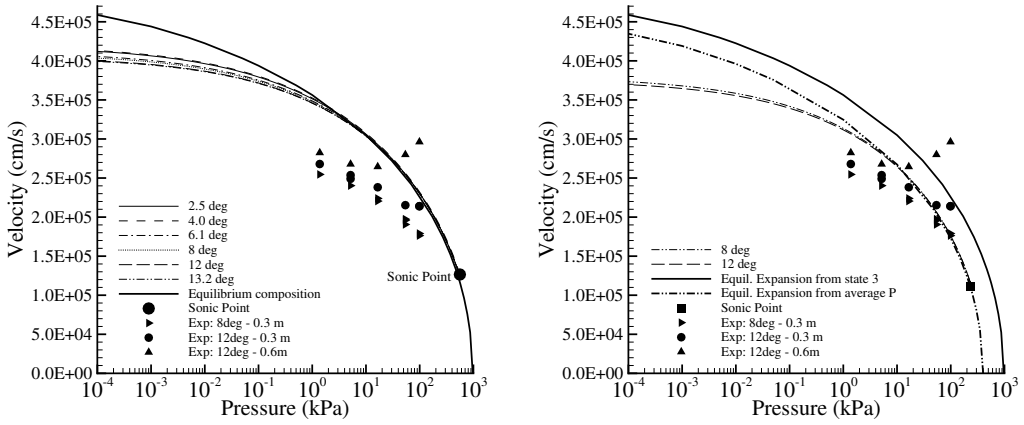


**Figure 17. (a) Steady flow predictions of velocity as a function of pressure. Also plotted are the experimental data of exhaust velocity calculated with Eq. 3. (b) Equilibrium and finite rate calculations starting from an average tube pressure of 400 kPa compared with equilibrium calculations starting from the state 3 pressure of 970 kPa.**

It is important to note that the pressure-area ratio relationship of Fig. 19 is for a nozzle inlet pressure equal to the average tube pressure. Near the end of the blowdown process the actual nozzle inlet pressure may be sufficiently lower than the average pressure such that Fig. 19 is no longer valid. Instead, the curve will be shifted to lower pressures increasing the likelihood that separation will occur and move closer to the nozzle inlet. As the tube pressure continues to decrease, the separation point will travel closer to the nozzle throat. When the separation point passes through the nozzle inlet, unchoking occurs and the flowfield becomes entirely subsonic. This event is assumed to occur late in the blowdown process.

For the initial times when Fig. 19 applies, the 8°-0.3 m nozzle is expected to separate when operated in environment pressures of 54.5 kPa and greater. For all environment pressures below 54.5 kPa, Fig. 19 predicts that no separation will occur. These same results are also valid for the shorter 12° nozzle. The longer 12° nozzle is expected to separate when operated in all environment pressures greater than 5.2 kPa. Only at the two lowest environment pressures tested of 5.2 and 1.4 kPa is separation not expected for this largest nozzle.

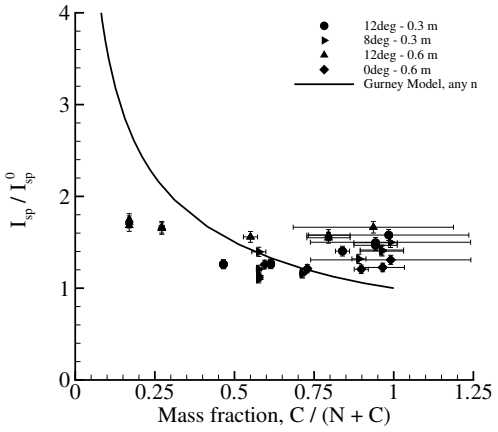


**Figure 18. Normalized specific impulse as a function of the explosive mass fraction. The Gurney model (see Cooper[2]) is plotted with the experimental data for tubes with nozzles.**

Overexpansion of the flow is predicted for the 12°-0.3 m nozzle exhausting into $P_0 = 16.5$ kPa and for the 12°-0.6 m nozzle exhausting into $P_0 = 5.2$ kPa. This is observed by comparing the predicted nozzle exhaust pressure (indicated by the solid dots in Fig. 19) to the environment pressure $P_0$ and to the expected separation pressure $0.4 \times P_0$. If the predicted nozzle exit pressure lies between $P_0$ and $0.4 \times P_0$ then the flow overexpands in the nozzle. Overexpansion of the flow is not desirable because the established pressure differential across the nozzle walls generates a force in the opposite direction of the pressure differential across the thrust surface. For this reason, separation within

the nozzle is often preferred. Sutton[19] states that nozzles with high area ratios that are typically designed for high altitude flight actually have a larger thrust when operated at sea level when separation is present than when operated at the design altitude. This similar effect is observed in the experimental data (Fig. 7) for the 12°-0.6 m nozzle where the impulse at 100 kPa is an average of 300 s while at $P_0 = 5.2$ kPa the impulse is 275 s. However, when the flow is highly separated, a large portion of the nozzle is not utilized so flight performance will suffer due to the additional engine weight and size.

### E. Startup time

The nozzle startup time is defined as the time from when the transmitted shock wave enters the nozzle throat until time when quasi-steady flow is established. The presence of this transient nozzle flow has previously been studied in shock tunnels and rocket nozzles. Observations of the nozzle starting process were recorded in images taken by Amann[17] and Smith[18] in reflected shock tunnels. Successive shadowgraph images were used to measure the wave trajectories in the experiments of Amann.[17] The experiments were carried out in two-dimensional reflection nozzles with a 15° half angle and a Mach 3 incident shock. Schlieren images of Smith[18] were taken downstream of the nozzle exit in an axisymmetric reflection nozzle with a 10° half angle with an incident shock wave of Mach 3.0 and 5.7. Wave trajectories were measured with thin-film heat transfer gauges and a pitot pressure gauge. In a more recent study by Saito and Takayama,[22] double exposure laser holographic interferometry was used to visualize the flow of a Mach 2.5 incident shock wave within a 15° half angle, two-dimensional reflection nozzle.

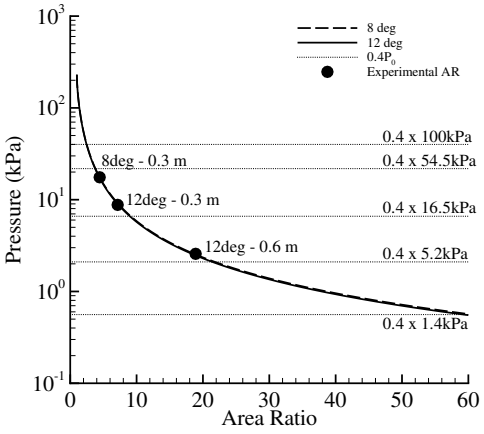


**Figure 19. Pressure decay in nozzles assuming steady flow and comparisons to the expected separation pressure in the experimental tests.**

The starting processes observed in the nozzles were qualitatively similar in each study. Three important features observed in these flows are the primary shock, the secondary shock, and the contact surface. AMRITA simulations carried out with a Mach 3 incident shock wave and a 15° half angle nozzle illustrate these features (Fig. 20).

(a) (b) (c)

**Figure 20. Frames from AMRITA inviscid simulation of starting process in a 15° half angle nozzle with an incident Mach 3 shock wave. Features to note are the primary shock, contact surface, secondary shock, and oblique expansions at the throat.**

The transmitted primary shock and contact surface propagate through the nozzle with a decreasing velocity as a result of the divergent cross section. Expansion fans originate behind the transmitted shock

at the corners of the nozzle inlet and reflect on the nozzle axis. A secondary shock wave forms between the contact surface and nozzle inlet. This left-facing shock wave moves upstream relative to the fluid and is needed to match the high Mach number, low pressure flow exhausting from the inlet to the low Mach number, high pressure flow behind the primary shock. A model and subsequent calculation using the method of characteristics by Smith[18] identifies that an unsteady expansion must exist downstream of the nozzle inlet. Because the primary shock and contact surface decelerate, the characteristics in the post-shock flow rotate and become convergent resulting in the formation of the secondary shock at the tail of the unsteady expansion. Successful starting of the nozzle and the establishment of quasi-steady flow occurs when this secondary shock is swept downstream and out of the nozzle . Failure of the nozzle to start occurs when the flow velocity coming from the inlet is not sufficient to prevent the secondary shock from reaching the nozzle inlet; the condition of sonic flow no longer exists at the throat and the downstream portion of the nozzle flow is completely subsonic.

Viscosity has also been shown to effect this starting process. The inviscid simulations of Igra et al.[23] accurately model the experiments of Amann[17] which lead them to conclude that the short startup time of their situation is not significantly affected by viscosity. However, in the experiments of Amann[17] and Saito and Takayama[22] which were also numerically simulated by Saito and Takayama[22] and Tokarcik-Polsky and Cambier,[24] the secondary shock wave was observed to bifurcate at the wall creating a region of separated flow. While the numerical simulations correctly predicted the shock bifurcation at the wall, the downstream region of separated flow was not accurately modeled. This was attributed to the use of a laminar boundary layer model in the simulations. A Reynolds number calculation by Saito and Takayama[22] suggests that the boundary layer is actually turbulent.

While shock tunnel experimenters strove to reduce the nozzle start time in order to maximize the test time, rocket nozzle developers sought to reduce the nozzle start time in order to prevent structural damage.[25] Flow instabilities during engine startup and shutdown generate large pressure fluctuations along the nozzle walls that can ultimately damage the nozzle. The flow transient during rocket engine startup is different than that of shock tunnel startup. During rocket engine startup at sea level, the pressure ratio across the nozzle increases as the combustion chamber increases to its steady state operating value. The rate of this pressure increase affects the startup process. If this process occurs instantaneously, we would expect the starting process to be closer to that of a shock tunnel nozzle discussed previously. For these flows in rocket engine nozzles during startup, the effect of viscosity is substantial. Numerical simulations by Chen et al.[25] of the startup of 1/16-scale nozzle of a J-2S rocket engine using a time-accurate compressible Navier Stokes solver with a turbulence model predict the ratio of wall pressure to chamber pressure over the nozzle length for a range of nozzle pressure ratios. In these cases, the predicted point of flow separation at the wall strongly agrees with the experimental data and occurs near the nozzle inlet.

For detonation tube nozzle flows, the startup process is certainly affected by viscosity at the low pressure ratios and is likely to also be affected by the Taylor wave pressure profile that exists behind the shock wave after it just enters the nozzle inlet. For simplicity, an estimate of the detonation tube nozzle startup time is made from the time taken by a particle as it travels under steady flow conditions from the inlet to the nozzle exit. The startup time is assumed to equal three durations of this steady flow time which is then compared to the total single-cycle time of the detonation tube. The experimentally measured time duration from ignition to the end of the blowdown process is approximately 4000 $\mu$s for the 8°-0.3m nozzle, 4500 $\mu$s for the 12°-0.3m, 5000 $\mu$s for this 12°-0.6m. Three durations of the steady flow time determined from the previous finite rate calculations yield values of approximately 252 $\mu$s for the 8°-0.3m nozzle, 354 $\mu$s for the 12°-0.3m, 642 $\mu$s for this 12°-0.6m nozzle. Thus, the startup time is expected to range between 6% and 12% of the total cycle time. Visualization experiments or numerical simulations are required to better estimate the effect of viscosity and the nozzle flow field in order to obtain more reasonable estimates of the startup time as a function of the environment pressure.

Multi-cycle operation would reduce this nozzle startup time and also reduce the amount of pressure decay experienced at the end of each cycle such that the average exhaust velocity would be greater than in the single-cycle case. As a result, the performance would likely increase closer to the theoretical steady flow

predictions.

### F. Comparison of experiments and steady flow analysis

With calculation of the effective nozzle inlet state, the specific impulse from the predicted exhaust velocity is determined using Eq. 3. This is plotted with all experimental data for tubes with and without a nozzle as a function of the pressure ratio across the nozzle ($P_3/P_0$ for the detonation tube data and $P_i/P_x$ for the steady flow predictions). The steady flow predictions are shown both for the nozzle inlet state based on state 3 (Fig. 17a) and for the nozzle inlet state based on the average pressure during the cycle (Fig. 17b).

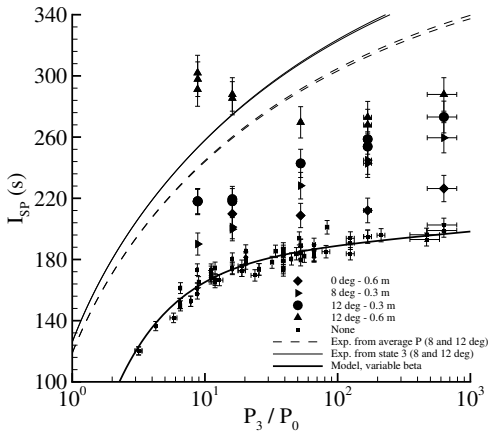


**Figure 21. Specific impulse as a function of the nozzle pressure ratio. The steady flow predictions based on isentropic expansion are also plotted.**

## V. Performance Implications

For pressure ratios $P_3/P_0$ greater than 100, no partial fill effects are observed and the data is best modeled assuming steady nozzle flow. It is of interest to determine the flight operating conditions that correspond to this pressure ratio. In the experiments, decreasing the environment pressure simulates an increase in altitude $P \sim \exp(-gy/RT)$. Because these experiments were carried out under static conditions, the experimental environment pressure $P_0$ represents the stagnation pressure for any given flight speed. The environment pressure for a given flight condition is determined from the isentropic relation for pressure as a function of Mach number.

$$(P_0)_{exps}/(P_0)_{flight} = [1 + 1/2(\gamma - 1)M^2]^{\gamma/(\gamma-1)} \tag{19}$$

Figure 22 plots the pressure ratio $P_3/P_0$ as a function of altitude for the static case and Mach numbers between 1.0 and 4.0. Thus, for the static case, $P_0$ refers to the stagnation pressure and for cases where $M \geq 1$, $P_0$ refers to the environment pressure at the flight conditions. Also plotted on Fig. 22 is a dotted line at a pressure ratio of 100 separating the flight conditions where the tamping and partial fill effects dominate the impulse and where quasi-steady expansion within the nozzle dominate the impulse. For example, for Mach 4.0 flight at an altitude of 9,144 m (30,000 ft), the nozzle pressure ratio is 4,303. This pressure ratio is sufficiently high such that the impulse is best predicted assuming steady flow within the nozzle. Predictions by Wintenberger[26] have indicated that the best performance of an air-breathing pulse detonation engine occurs between Mach 1.0 and 2.0. For this range of Mach numbers, both nozzle operating regimes may exist until the altitude exceeds approximately 14,000 m (∼46,000 ft). Thus, the nozzle pressure ratio at flight conditions should be carefully considered when making predictions of the impulse.

## VI. Summary and Conclusions

Experiments were carried out to measure the impulse from detonation tubes with exit nozzles as a function of the environment pressure. Adding a nozzle onto the tube was found to increase the impulse over the case of a tube without a nozzle at all the environment pressures. Observations of the experimental data determined that the partial fill effect dominates the impulse for the largest environment pressures tested and that this effect decreases as the tamper mass and environment pressure decrease. In this case, a straight extension is more effective at increasing the impulse than a diverging nozzle for tubes with equivalent explosive mass

fractions. At the lowest environment pressures, quasi-steady flow is established within the nozzle and the effect of the nozzle divergence expands the flow. In this case, a diverging nozzle is more effective at increasing the impulse over a straight extension.

To better understand the effect of nozzles on detonation tubes at low environment pressures, the experimental data was analyzed assuming that quasi-steady flow was established in the nozzle. This modeling is reasonable when the environment pressure is sufficiently low such that separation does not occur in the nozzle and the startup time is only a small fraction of the entire blowdown time. Because the detonation tube pressure upstream of the nozzle inlet decreases in time, the average tube pressure from which to determine the nozzle inlet condition was found to best represent the experimental data. Comparisons of the steady flow nozzle predictions based on the average detonation tube pressure modeled the data for all of the diverging nozzles at the lowest environment pressures. The steady flow predictions did not model the data for the larger nozzles at the largest environment pressures due to the influence of the tamper mass.

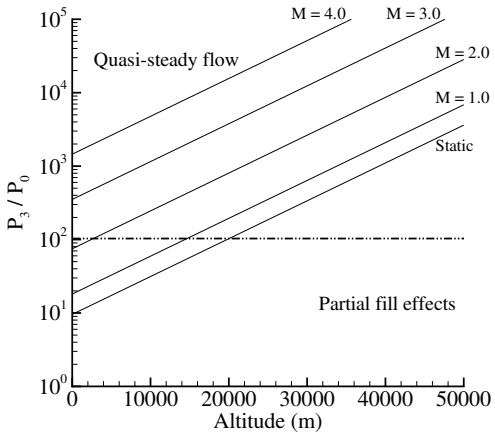


**Figure 22. Nozzle pressure ratio as a function of flight Mach number and altitude.**

Thus, nozzles on detonation tubes have been shown to increase the impulse over the baseline case of a plain tube but their performance depends on the pressure ratio across the nozzle and the nozzle shape. Large nozzles operating under small initial pressure ratios are in the regime where unsteady gas dynamics and the partial fill effects of the tamper mass are important. This effect is of decreasing importance as the nozzle size is reduced. All nozzles operating under large initial pressure ratios are in the regime where quasi-steady flow exists in the nozzle and the usual steady flow analysis techniques can be used to predict upper bounds to the performance.

## VII. Acknowledgments

This work was supported by the Office of Naval Research Grant *Pulse Detonation Engines: Initiation, Propagation, and Performance* (Dept. of Navy Grant number N00014-02-1-0589, subcontract PY-1905).

## References

[1]Wintenberger, E., Austin, J., Cooper, M., Jackson, S., and Shepherd, J. E., "An Analytical Model for the Impulse of a Single-Cycle Pulse Detonation Engine," *Journal of Propulsion and Power*, Vol. 19, No. 1, 2003, pp. 22–38.

[2]Cooper, M. A., *Impulse generation by detonation tubes*, Ph.D. thesis, California Institute of Technology, Pasadena, California, 2004.

[3]Cambier, J. L. and Tegner, J. K., "Strategies for Pulsed Detonation Engine Performance Optimization," *Journal of Propulsion and Power*, Vol. 14, No. 4, 1998, pp. 489–498.

[4]Eidelman, S. and Yang, X., "Analysis of the Pulse Detonation Engine Efficiency," 34th AIAA/ASME/SAE/ASEE Joint Propulsion Conference and Exhibit, July 13–15, 1998, Cleveland, OH, AIAA 98–3877.

[5]Yang, V., Wu, Y. H., and Ma, F. H., "Pulse Detonation Engine Performance and Thermodynamic Cycle Analysis," ONR Propulsion Meeting, 2001.

[6]Guzik, S., Harris, P. G., and Champlain, A. D., "An investigation of pulse detonation engine configurations using the method of characteristics," 38th AIAA/ASME/SAE/ASEE Joint Propulsion Conference and Exhibit, July 7-10, 2002, Indianapolis, IN, AIAA2002-4066.

[7]Harris, P. G., Guzik, S., Farinaccio, R., Stowe, R. A., Whitehouse, D., Josey, T., Hawkin, D., Ripley, R., Link, R., Higgins, A. J., and Thibault, P. A., "Comparative Evaluation of Performance Models of Pulse Detonation Engines," 38th AIAA/ASME/SAE/ASEE Joint Propulsion Conference and Exhibit, Indianapolis, IN, 2002-3912.

[8]Morris, C. I., "Numerical modeling of pulse detonation rocket engine gasdynamics and performance," 42nd AIAA

Aerospace Sciences Meeting and Exhibit, Reno, NV, January 5–8, 2004–0463.

[9]Cooper, M., Jackson, S., Austin, J., Wintenberger, E., and Shepherd, J. E., "Direct Experimental Impulse Measurements for Detonations and Deflagrations," *Journal of Propulsion and Power*, Vol. 18, No. 5, 2002, pp. 1033–1041.

[10]Falempin, F., Bouchaud, D., Forrat, B., Desbordes, D., and Daniau, E., "Pulsed Detonation Engine Possible Application to Low Cost Tactical Missile and to Space Launcher," 37th AIAA/ASME/SAE/ASEE Joint Propulsion Conference and Exhibit, July 8–11, 2001, Salt Lake City, UT, AIAA 2001–3815.

[11]Allgood, D. and Gutmark, E., "Effects of exit geometry on the performance of a pulse detonation engine," 40th AIAA Aerospace Sciences Meeting and Exhibit, January 14–17, Reno, NV, AIAA2002-0613.

[12]Allgood, D., Gutmark, E., Rasheed, A., and Dean, A. J., "Experimental investigation of a pulse detonation engine with a 2D ejector," 42nd AIAA Aerospace Sciences Meeting and Exhibit, January 5–8, Reno, NV, AIAA2004-0864.

[13]Tzuk, Y., Bar, I., and Rosenwaks, S., "Dynamics of the detonation products of lead azide. IV. Laser shadowgraphy of expanding species," *J. Appl. Phys.*, Vol. 74, No. 9, 1993, pp. 5360–5365.

[14]Grigor'ev, V. V., "Use of a Nozzle in Particle Acceleration by a Flow of Gas Detonation Products in Tubes," *Combustion, Explosion, and Shock Waves*, Vol. 32, No. 5, 1996, pp. 492–499.

[15]Thomas, G. O. and Williams, R. L., "Detonation interaction with wedges and bends," *Shock Waves*, Vol. 11, 2002, pp. 481–492.

[16]Akbar, R., Schwendeman, D. W., Shepherd, J. E., Williams, R. L., and Thomas, G. O., "Wave shaping channels for gaseous detonations," *Shock Waves at Marseille IV*, edited by R. Brun and L. Z. Dumitrescu, Springer-Verlag, Berlin, 1995.

[17]Amann, H. O., "Experimental study of the starting process in a reflection nozzle," *The Physics of Fluids Supplement*, Vol. I, 1969, pp. 150–153.

[18]Smith, C. E., "The starting process in a hypersonic nozzle," *J. Fluid Mechanics*, Vol. 24, 1966, pp. 625–640, part 4.

[19]Sutton, G. P., *Rocket Propulsion Elements*, John Wiley and Sons, Inc., New York, NY, sixth ed., 1992.

[20]Reynolds, W. C., "The Element Potential Method for Chemical Equilibrium Analysis: Implementation in the Interactive Program STANJAN, Version 3," Tech. rep., Dept. of Mechanical Engineering, Stanford University, Stanford, CA, January 1986.

[21]Scofield, M. P. and Hoffman, J. D., "Maximum thrust nozzles for nonequilibrium simple dissociating gas flows," *AIAA Journal*, Vol. 9, No. 9, 1971, pp. 1824–1832.

[22]Saito, T. and Takayama, K., "Numerical simulations of nozzle starting process," *Shock Waves*, Vol. 9, 1999, pp. 73–79.

[23]Igra, O., Wang, L., Falcovitz, J., and Amann, O., "Simulation of the starting flow in a wedge-like nozzle," *Shock Waves*, Vol. 8, 1998, pp. 235–242.

[24]Tokarcik-Polsky, S. and Cambier, J., "Numerical study of transient flow phenomena in shock tunnels," *AIAA J.*, Vol. 32, No. 5, 1994, pp. 971–978.

[25]Chen, C. L., Chakravarthy, S. R., and Hung, C. M., "Numerical investigation of separated nozzle flows," *AIAA Journal*, Vol. 32, No. 9, 1994, pp. 1836–1843.

[26]Wintenberger, E., *Application of steady and unsteady detonation waves to propulsion*, Ph.D. thesis, California Institute of Technology, 2004.